♦ The Quantum Cascade Laser: A Versatile High-Power Semiconductor Laser for Mid-Infrared Applications

Oana Malis, Claire Gmachl, Deborah L. Sivco, Loren N. Pfeiffer, A. Michael Sergent, and Kenneth W. West

Since its invention at Bell Labs in the mid-nineties, the quantum cascade laser (QCL) has evolved rapidly to become a viable commercial alternative to other solid-state mid-infrared light sources. QCLs are compact, high-power, wavelength-agile laser devices that are ideally suited for mid-infrared applications such as chemical sensing and free-space telecommunications. This paper summarizes our recent progress in QCL technology, with a particular emphasis on device design and fabrication. The current state-of-the-art in performance of InP lattice-matched QCL is reviewed. In order to expand the functionality of QCLs, new materials and device concepts are being explored. In particular, nonlinear light generation in QCLs is discussed in detail. The experimental results confirm the potential of nonlinear QCLs to extend the wavelength range of InP-based devices. Ongoing efforts to improve the fabrication of InP-based QCLs and to develop new QCL materials are presented.

Introduction

Quantum cascade lasers (QCLs) are compact, rugged, high-power, semiconductor light sources operating in the mid- to far-infrared range of the spectrum. Unlike quantum-well semiconductor lasers, QCLs can be designed to operate at any wavelength within a broad spectral range. While QCL emission has been demonstrated down to the terahertz range, this paper will focus on mid-infrared Type I QCLs. In the approximately ten years since its invention at Bell Labs [11], QCL technology has evolved rapidly and has been extremely helpful in extending our knowledge of semiconductor physics. Moreover, the swift development of QCLs has led to a technology transfer from research to production; mid-infrared QCLs are currently offered commercially by several Lucent licensees. This rapid progress was made possible not only by the extremely active worldwide research on band-engineering, but also by the continuous development of molecular beam epitaxy (MBE), the semiconductor growth technique that enables accurate nanometer control and the reproducibility of complex semiconductor structures. Today, QCL technology promises to have a major impact in fields ranging from chemical sensing to free-space telecommunications.

This paper presents an overview of QCL technology, with a particular focus on current research activities at Bell Labs. First, the principles of QCL operation are introduced. Then, material growth,

Bell Labs Technical Journal 10(3), 199–214 (2005) © 2005 Lucent Technologies Inc. Published by Wiley Periodicals, Inc. Published online in Wiley InterScience (www.interscience.wiley.com). • DOI: 10.1002/bltj.20114

device processing, and device characterization are discussed in detail. Next, current state-of-the-art device performance is presented and the factors limiting device performance are investigated. It turns out that QCL light characteristics and operating range are limited by some fundamental properties of the materials of choice. A separate section is devoted to ongoing research efforts at Bell Labs to push the limits of QCL operation and to explore new materials and device concepts. The following section briefly discusses applications of QCLs. The final section presents some concluding remarks and offers a perspective on future research and development.

Panel 1. Abbreviations, Acronyms, and Terms

CVD—Chemical-vapor deposition
cw—Continuous wave
DFB—Distributed feedback
DIAL—Differential-absorption LIDAR
epi—Epitaxial
HR—High reflectance
L-I—Output versus current
LIDAR—Laser radar
LO—Longitudinal optical
MBE—Molecular beam epitaxy
MOCVD—Metal-organic chemical-vapor deposition
ppb—parts per billion
QCL—Quantum cascade laser
QW—Quantum wells
RADAR—Radio detection and ranging
SH—Second harmonic
TEM—Transmission electron microscopy
TILDAS—Tunable infrared laser diode absorption spectroscopy
TM—Transverse magnetic
VCSEL—Vertical cavity surface-emitting lasers

QCL Principles of Operation

QCLs are unipolar semiconductor devices consisting of complex layered structures of two or more semiconductor alloys [11, 15]. **Figure 1** shows a laser bar containing several QCLs mounted on a copper heat-sink (a), an scanning-electron microscopy (SEM) image of an individual laser device (b), and a transmission electron microscopy (TEM) image of the semiconductor layered structure inside the active waveguide core of the device (c). The light is generated in the active region by an intersubband transition of the single charge carriers (i.e., the electrons) between two quantized levels in the conduction band. Because the energy difference between the two quantized levels is determined by the specific structure design (i.e., the quantum well [QW] and barrier widths), the wavelength emitted can be tailored by band-engineering to be any value within a broad spectral range. This range is limited only by the conduction-band offset available between the two materials of choice and the Reststrahlen region.

This section will be using InP lattice-matched alloys to exemplify the QCL principles of operation, but the general concepts are the same for any other material system. In InP-based QCLs, the active region consists of $In_{0.53}Ga_{0.47}As$ QWs and $In_{0.52}Al_{0.48}As$ barriers (see Figure 1c). The conduction-band offset for these two materials is 0.52 eV at low temperatures and corresponds to an operation range between 5 μm and 20 μm. It is noteworthy that QCL operation has also been achieved in strained InGaAs/InAlAs devices on InP as well as in GaAs/AlGaAs and Sb-based material systems. **Figure 2** shows the detailed band structure of a QCL biased at operating voltage. In this basic design, the active region of the device consists of three strongly coupled QWs. The light is emitted by a transition between levels 3 and 2. In order to achieve population inversion for lasing, the electrons must be injected rapidly into the upper level 3 and then rapidly extracted from level 2. Fast depopulation of level 2 is achieved by means of longitudinal-optical (LO) phonon scattering from level 2 into level 1, which is located approximately 35 meV below level 2. The injector region, here consisting of 5 QWs, has the role of facilitating the transport of the electrons through the device by insuring fast extraction from both level 1 and level 2 and fast re-injection into level 3 of the down-stream active region. To maximize the gain, 30 to 100 active regions are typically chained (i.e., "cascaded") together. The electrons are recycled from one active region to the next, emitting more than one photon per pass through the device. This process is the reason for the high emission power of these devices.

The basic QCL structure exemplified in Figure 2 has evolved over the years into many more sophisticated designs. The three-level active region can be

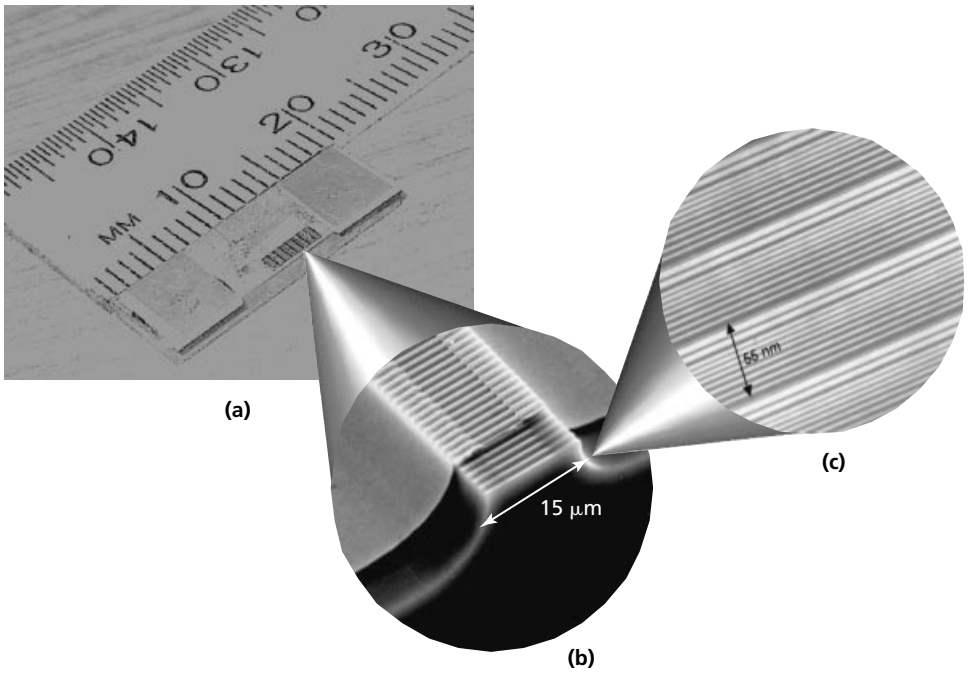

DFB-QCL—Distributed feedback-quantum cascade laser
QCL—Quantum cascade laser
SEM—Scanning electron microscopy
TEM—Transmission electron microscopy

(a) QCL bar containing several devices mounted on a copper heat-sink and wire-bonded to Au-plated alumina contact pads
(b) SEM image of the front facet portion of a deep-etched ridge-waveguide DFB-QCL
(c) TEM image of a portion of the active waveguide core of a QCL

Figure 1.
The quantum cascade laser is a compact, rugged, high-power, semiconductor light source.

replaced by a superlattice to allow large current-carrying capabilities [40]. In this case, the lasing transition occurs between two extended states of the superlattice minibands. If the transition is between a localized state and an extended superlattice state, the design is referred to as a bound-to-continuum transition [9]. Moreover, the transition can be either vertical, as in the above examples, or diagonal, a design that increases the upper-laser-state lifetime [10].

Using the usual rate-equation formalism, the material gain coefficient can be calculated as [15]

$$g = \tau_3\left(1 - \frac{\tau_2}{\tau_{32}}\right)\frac{4\pi e z_{32}^2}{\lambda \varepsilon_0 n_{ef} L_p}\frac{1}{2\gamma_{32}},$$

where τ_3 is the total upper-state lifetime, τ_2 the total lifetime of level 2, τ_{32} the lifetime of the 3-2 transition, Z_{32} the matrix dipole moment for the 3-2 transition, n_{ef} the effective refractive index at wavelength λ, L_p the thickness of one active region and injector, ε_0 the vacuum dielectric constant, e the elementary charge, and $2\gamma_{32}$ the full width at half maximum of the luminescence spectrum. The lifetimes are determined by LO-phonon interband scattering and are of the order of ps.

Laser action requires that the material gain overcome the device losses. The losses come from two main sources: the nonresonant free-carrier losses in the waveguide, α_w, typically calculated with a Drude model, and the mirror losses, α_m, given by $\alpha_m = (1/L)\ln(R)$, where R is the mirror reflectivity $R = ((n-1)/(n+1))^2$. The threshold current density J_{th} is then given by

$$J_{th} = \frac{\alpha_m + \alpha_w}{g\Gamma},$$

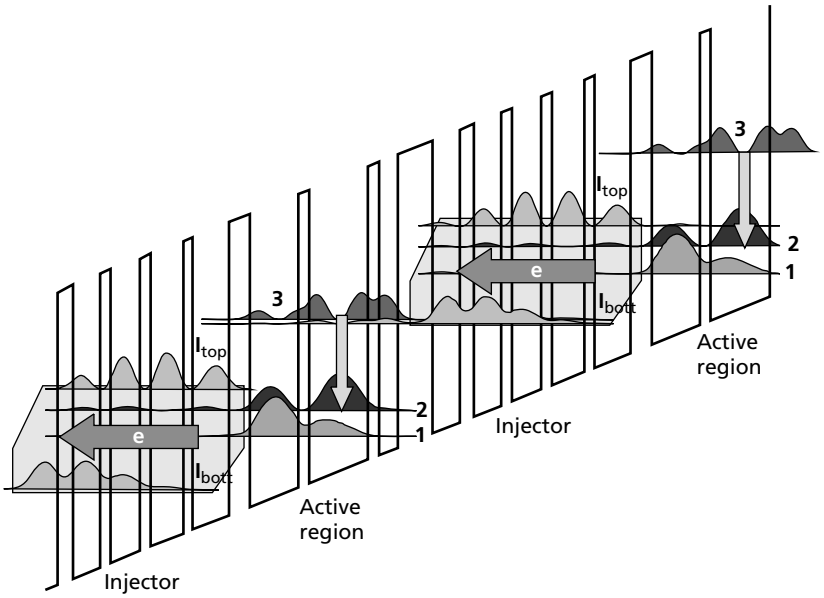

The laser transition is indicated by the arrow between levels 3 and 2. The layer thicknesses in nanometers of one period of active material and injector are, from right to left starting from the injection barrier: **3.8**/2.1/**1.2**/6.5/**1.2**/5.3/**2.3**/*4.0*/***1.1***/*3.6*/***1.2***/*3.2*/***1.2***/*3.0*/***1.6***/*3.0*. The underlined layers are n-type doped. The barriers are indicated in bold symbols; italic style shows the injector region. The applied electric field is 65 kV cm^{-1}.

Figure 2.
Conduction band diagram of the active and injector regions of an 8 μm QCL and the moduli squared of the most significant wavefunctions.

where Γ is the confinement factor, typically of the order of 0.5. For the structure in Figure 2, the losses can be estimated as $\alpha_m = 5.1\ cm^{-1}$ (for a 2.5 mm-long cavity) and $\alpha_w = 19\ cm^{-1}$, resulting in a threshold current density of 1.6 kA/cm^2. This typical value for a three-well design emphasizes the main limiting aspects of QCL devices, i.e., their high threshold and operating currents.

In order to minimize device losses and confine the mid-infrared light to the gain material, the active region is inserted into a waveguide. **Figure 3** shows the structure of a typical QCL waveguide, together with the profiles of the refractive index and of the lowest-order transverse-magnetic mode (TM_{00}). The waveguide core consists of the active section stacked between two InGaAs layers. The claddings are given on one side by the InP substrate and on the other by either an InAlAs or another InP layer. A highly-doped plasmon-enhanced InGaAs layer also contributes to the confinement. The thicknesses and doping profiles of the various waveguide layers depend on the specific application. The waveguide in Figure 3 is optimized for low loss and maximum overlap of the TM_{00} mode with the active region.

The dielectric waveguide shown in Figure 3 is a Fabry-Perot-type resonator that emits a multimode laser spectrum. For certain applications, however, it is desirable to have single-mode operation. This is achieved with a distributed feedback (DFB) resonator. A DFB resonator consists of a grating of period $\Lambda = \lambda_B/(2 \cdot n_{eff})$ etched in the top cladding of the device. For practical processing reasons, DFB top claddings are typically significantly thinner than that shown in Figure 3. The grating induces a modulation in the refractive index and losses along the laser ridge that selects a unique emission wavelength for each lateral and transverse mode of the cavity. Because the refractive index depends on temperature, the QCL wavelength also varies with temperature. QCL temperature tunability, which is particularly important

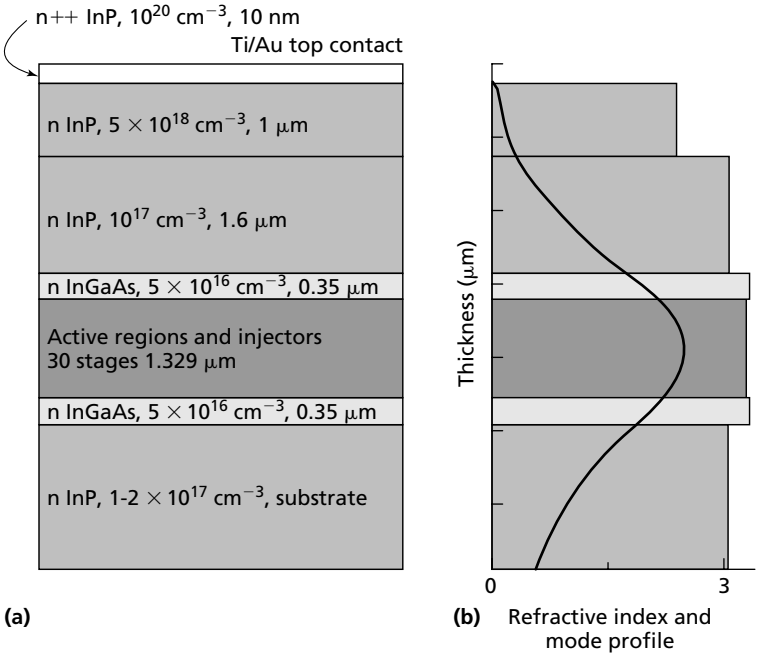

QCL—Quantum cascade laser
TM—Transverse magnetic

(a) Layer structure of a low-loss waveguide for the 8 μm QCL shown in Figure 2
(b) The corresponding profiles of the refractive index and magnetic field of the TM_{00} mode

Figure 3.
Waveguide structure of a QCL.

for spectroscopy applications, is achieved by changing the active region temperature by adding a DC ramp to the laser current drive.

QCL Material Growth

The complex QCL structures are grown by solid-source MBE on n-type InP (100) substrates doped at the level of $1–2 \cdot 10^{17}/cm^3$. MBE has so far proven to be the growth technique of choice, because it allows accurate control of sub-nanometer size semiconductor layers. Moreover, MBE has high reproducibility over the entire structure, which may be 5 μm to 10 μm thick and contain more than 500 layers. Figure 1c shows the TEM image of several active regions of a QCL structure. The growth of InP lattice-matched materials is extremely demanding and requires precise control of the InGaAs and InAlAs alloy composition. The MBE-grown structures are characterized using x-ray scattering for the alloy composition and Hall measurements for doping calibration. It is worth noting that QCLs have also been successfully grown by metal-organic chemical-vapor-deposition (MOCVD) [35, 20].

For InP-containing structures, such as InP top-cladding devices, we have been using a two-step MBE growth process. First, the P-free core of the device is grown in an arsenide machine and the material is capped with a low-temperature, pure As layer. Then, the sample is transferred into a second MBE machine equipped with a solid P-source and the top InP-containing layers are grown. InP has the advantage of having lower mid-infrared losses and a lower refractive index than InAlAs as well as higher thermal conductivity. This results in a better optical confinement of the wave and ultimately in improved laser performance. The two-step technique has been most

successful in growing buried-grating DFB lasers. To improve the thermal properties of the devices, we have also used InP overgrowth by MOCVD; this technique will be discussed in detail in the following sections.

QCL Device Processing

The QCL devices are typically processed into 4 μm to 16 μm wide, 0.5 mm to 3 mm long, deep-etched ridge-waveguide lasers (Figure 1b). First, using standard photo-lithography, the laser mesas are defined using either chemical wet-etching or dry-etching. Then, the insulator Si_3N_4 or SiO_2 is deposited using chemical-vapor deposition (CVD). GeSe chalcogenide has also been used as an insulator, because of its superior mid-infrared properties. In the next step, a window is opened into the insulator using freon plasma-etching to access the top of the mesa electrically, followed by thermal evaporation and the lift-off of the top Ti/Au contact. The wafer is thinned (i.e., lapped) to 200 μm before depositing the back Ge/Au/Ag/Au contact. The laser mirror facets are obtained by simply cleaving the device to the desired length. Metallic high-reflectance (HR) coatings on the back facets are also used to reduce the mirror losses. Finally, the as-cleaved or HR-coated devices are mounted with In on copper heat-sinks and wire-bonded to Au-coated alumina contact pads (Figure 1a).

DFB laser processing differs only slightly from this procedure. Before all the steps outlined above, the DFB grating is wet-etched across the entire sample; then the sample is processed in the normal way. The DFB grating is visible on the top of the ridge in Figure 1b. QCLs have also been processed into more sophisticated resonator designs, including micro-cavity lasers [12, 16] and photonic crystal lasers [4].

Device Characterization

The samples are measured on the temperature-controlled cold-finger of an He-flow cryostat at temperatures from 10 K to 300 K. The lasers are operated in either pulsed mode, with 50 ns to 100 ns current-pulse widths at repetition rates of 4 kHz and 84.2 kHz, or continuous-wave (cw) mode. The laser spectra are taken using a Nicolet Fourier Transform Infrared Spectrometer fitted with cooled HgCdTe and InSb detectors for the long- and short-wavelength ranges, respectively. The pulsed-light output versus current (L-I) measurements are taken with a calibrated fast HgCdTe photovoltaic detector for the laser light or a cooled InSb detector for the nonlinear light. The cw L-I measurements are taken with a calibrated power detector.

In **Figure 4**, 4a shows the pulsed L-I curves of a device with the active region detailed in Figure 2 emitting at 8 μm at temperatures between 5 K and 300 K. The peak power exceeds 1 W at cryogenic temperatures but decreases dramatically with increasing temperature to 500 mW at room temperature. The maximum peak power depends strongly on the number of active stages, as can be seen in the inset of Figure 4a.

QCLs based on the three-well structure discussed so far also operate in continuous-wave (cw) mode at low temperatures, as shown in Figure 4b. The maximum cw operating temperature is limited by the thermal properties of the package, which consists of the device and the holder. Because of the high laser-threshold currents and poor thermal conductivity of the deep-etched ridge-waveguide geometry, the temperature of the active region exceeds the heat-sink temperature by more than 100 K. As a result of this temperature run-off, the laser can never reach its threshold current above a certain heat-sink temperature. The next section will discuss in detail ongoing efforts in our group to overcome this effect. Using metal-buried heterointerfaces, Razeghi and her collaborators have achieved QCL cw operation at 6 μm up to 333 K and a power of 424 mW at 293 K with a plug efficiency of 3.2% [43, 8].

Ongoing Research at Bell Labs

The QCL research at Bell Labs is a multi-pronged effort focused on enhancing and expanding the mid-infrared functionality of these devices. This section briefly summarizes three directions of research and development. First, we are working to extend QCL functionality by means of nonlinear light-generation. Then, building on Bell Labs' world-renowned experience with material growth, we are exploring new

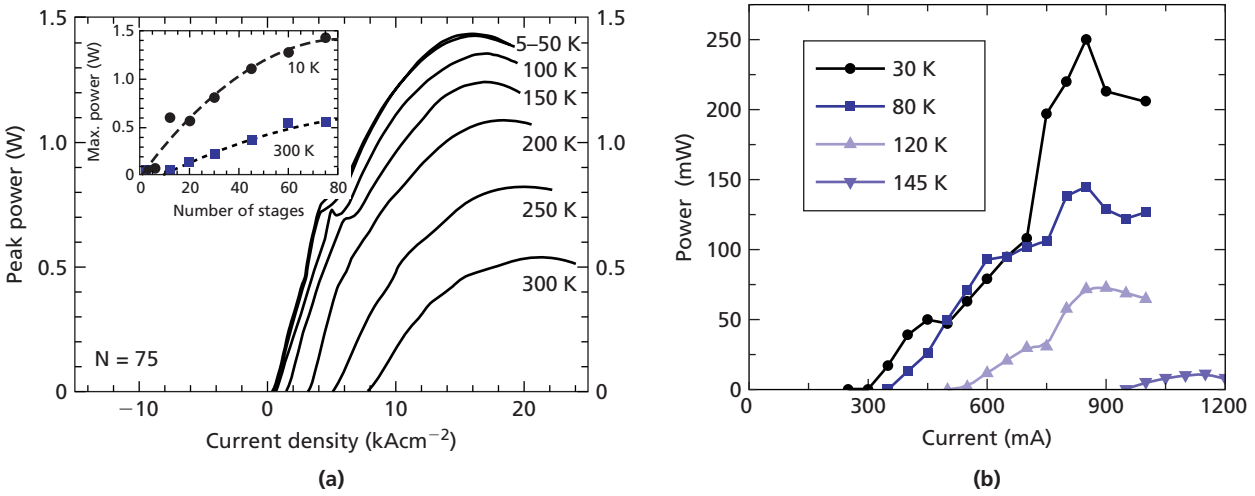

L-I—Output versus current
QCL—Quantum cascade laser

(a) Pulsed L-I curves of an 8 μm QCL with 75 stages of the active region shown in Figure 2 at temperatures from 5 K to 300 K. The inset shows the dependence of the maximum power on the number of stages at 10 K and 300 K. **(b)** Continuous-wave L-I plot of a 6 μm QCL at temperatures from 30 K to 145 K.

Figure 4.
QCL performance characterization in pulsed and continuous-wave operation modes.

material systems that would enable new QCL functionality. Finally, this exploration into new device and materials concepts is going on in parallel with a continuous effort to improve the performance of the more mature InP-based technology.

Nonlinear Quantum Cascade Lasers

QCLs operate in a broad mid-infrared spectral range, but, as pointed out above, for each material system, this range is limited by some fundamental property of the material (e.g., the conduction-band offset). Nonlinear light generation offers the potential of extending the functionality of QCLs beyond the limits set by the intrinsic properties of materials. Of particular technological interest is the low-wavelength spectral range below 5 μm, in which no clearly advantageous semiconductor laser technology has yet been identified. Nonlinear QCLs use the giant nonlinear properties of resonant intersubband transitions [3, 21]. These properties have been studied intensively over the past 20 years, but practical applications of them have been limited by the lack of compact, powerful pump sources and versatile phase-matching techniques. The first obstacle was recently overcome by monolithically integrating the nonlinear intersubband transitions with the structure of a QCL [32]. The idea of monolithically integrating nonlinear intersubband transitions with the QCL structure is natural, because they both use intersubband transitions to generate light. However, from a practical point of view, the strict current-injection requirements of these devices raise significant design challenges. Sum-frequency and second-harmonic (SH) generation were the first nonlinear processes demonstrated in QCLs [14, 32]. Third-harmonic generation has also since been reported [31].

We are currently investigating means to improve second-harmonic generation in QCLs [27, 28]. The first step was to design an active region that acts simultaneously as a pump source and a nonlinear mixing region. In **Figure 5**, 5a shows the detailed band structure of the optimized design. This structure exhibits a record-high nonlinear susceptibility of $|\chi^{(2)}| \sim 4 \times 10^{-5}$ esu (2×10^4 pm/V), a value that is at least three times higher than the values measured for any other material. The second step was to develop

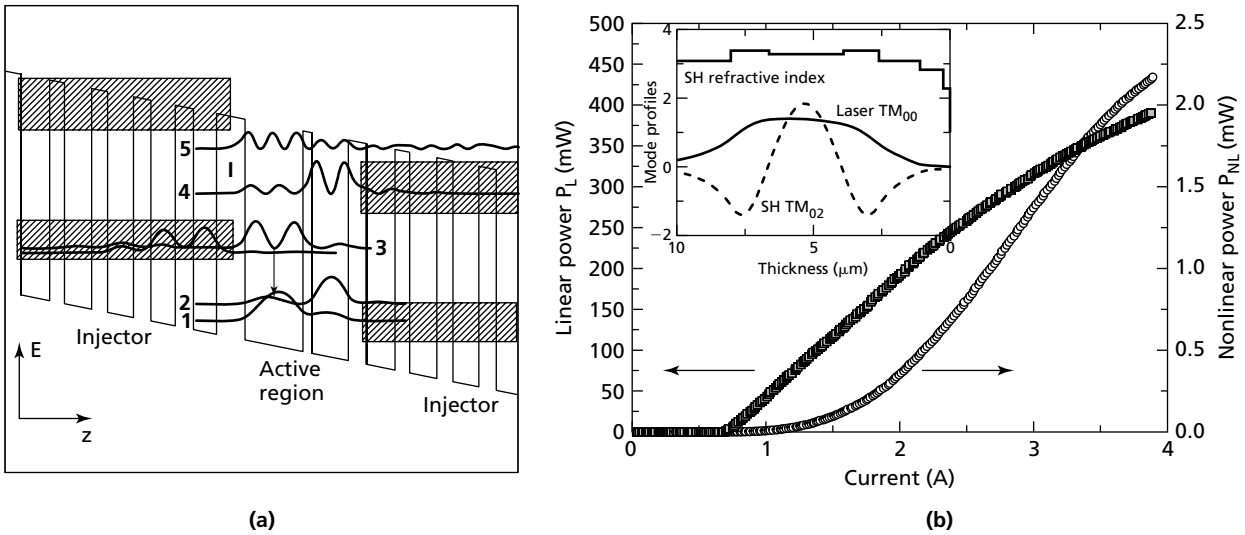

QCL—Quantum cascade laser
L-I—Output versus current
SH—Second harmonic
TM—Transverse magnetic

(a) Conduction band diagram of one QCL active region stacked between two injector regions of a structure optimized for second-harmonic generation and the moduli squared of the essential wavefunctions. The laser transition occurs between levels 3 and 2. The resonant intersubband cascades are 2 - 3 - 4 and 3 - 4 - 5. The dashed rectangles indicate the extent of the minibands inside the injector regions. The layer thicknesses of one period of active region-injector are from left to right starting at injection barrier "I": **4.1**/8.3/**1.3**/5.2/**2.6**/4.1/**2.1**/3.9/**2.3**/3.7/**2.5**/3.5/**2.6**/3.3 nm. The barriers are indicated by bold font, and the underlined layers are doped to 3.0×10^{17} cm^{-3}.
(b) Pulsed L-I curves for the laser and nonlinear light at 5 K for a device with the active region shown in **(a)**. The inset shows the profiles of the SH refractive index and the laser TM_{00} and SH TM_{02} modes for a phase-matching waveguide. The calculated refractive indices of the fundamental TM_{00} and SH TM_{02} modes for an infinitely wide waveguide are 3.2079 and 3.1689, respectively.

Figure 5.
Structure and performance of a nonlinear QCL emitting fundamental light at 9 μm and second-harmonic light at 4.5 μm.

a phase-matching technique between the fundamental and nonlinear light. We found that, due to the flexibility in the design of the QCL waveguide, modal-phase matching is the most promising candidate. Modal-phase matching consists in matching the effective refractive indices of the laser and nonlinear light of different order transverse modes. For the second-harmonic process, the laser TM_{00} mode and the SH TM_{02} mode offer the best choice in terms of refractive indices, lowest losses, and highest overlap with each other and with the active region. The inset of Figure 5b shows the profiles of these two modes together with the profile of the SH refractive index. An additional degree of freedom is given by the strong dependence of the refractive indices on the ridge-width. Using the active region of Figure 5a and including phase-matching considerations in the design of the waveguide, a record second-harmonic power of 2 mW was achieved at 4.55 μm (Figure 5b) [28]. This result was made possible by the use of an InP top-cladding waveguide and of HR coating on the laser back facets. We are currently working on lowering the SH emission wavelength below 4 μm and improving the thermal characteristics of the devices. We are also investigating other nonlinear processes, such as frequency down-conversion and coherent inversionless lasing [29].

Novel Materials

Another approach to expanding QCL functionality is to explore new material systems. The GaAs/AlGaAs system has been shown to be a potential competitor of InP lattice-matched materials [37]. This system is particularly attractive because it uses the

most mature III-V growth technology on a relatively cost-effective GaAs substrate. Unfortunately, GaAs QCLs suffer from the fact that AlGaAs is an indirect-gap semiconductor above about 45% Al composition. Once the minimum of the X-valley in the injection barrier becomes lower than the Γ-point upper-laser level, the device performance degrades rapidly [42]. This effect limits the operation wavelength of a GaAS QCL to the 8 μm to 20 μm range. In contrast to the conduction band, the valence band of the AlGaAs alloys has a maximum at the Γ-point throughout the compositional range. Therefore, a device using hole intersubband transitions in the valence band rather than electron intersubband transitions in the conduction band could take advantage of the full valence-band offset between pure GaAs and AlAs compounds. This valence-band offset (i.e., 0.51 eV) is comparable to the conduction-band offset in the InGaAs/InAlAs material system and would enable emission in a similar 5 μm to 20 μm mid-infrared range. Moreover, hole QCLs have the potential to allow the design of devices with new properties, such as surface-emitting QCLs and vertical cavity surface-emitting lasers (VCSELs).

Because of the complexities of the valence band, the hole intersubband transitions have not been studied as intensively as their electronic counterparts. Most of the investigations of intersubband transitions in the valence band have been done in p-type Si-SiGe QWs, in which intersubband absorption, electroluminescence, and photocurrent measurements have been reported [2, 5–7]. However, the Si-SiGe material system presents some significant theoretical and growth challenges associated with the built-in strain of these lattice-mismatched materials. The GaAs-AlGaAs system has the advantage of being virtually strain-free, and it is well understood from the material-growth point of view, but most of the research on this system has focused on infrared photodetectors [39].

As a first step toward a hole-based mid-infrared emitter, we are exploring the properties of inter-valence band transitions in GaAs QWs with high Al composition barriers. Bound-to-bound intersubband absorption in C-doped GaAs QWs was measured in the mid-infrared range. Taking advantage of a high-purity MBE facility at Bell Labs, GaAs QWs with modulation-doped $Al_{0.57}Ga_{0.43}As$ barriers were grown on (100) GaAs substrates. In order to reduce the interface roughness and to control the well dimensions with 1% accuracy, the QW widths were chosen to be exact integers of the monolayer spacing (i.e., 25.5, 31.13, 36.79, and 45.28 Å, corresponding to 9, 11, 13, and 16 monolayers, respectively). The high Al-composition AlGaAs is a digital alloy formed by a short-period superlattice of 11.3 Å AlAs and 8.5 Å GaAs. The QWs were modulation-doped with carbon, using a unique custom-made solid carbon source. Carbon is preferable to beryllium for p-type doping, because it has a lower diffusion constant at the MBE growth temperatures. The C-source we employed is compatible with very high purity GaAs material growth, as confirmed by mobility measurements of two-dimensional electron gasses. Using Hall measurements, the two-dimensional hole gas for the 31 Å QW sample was estimated to have a density of 1.6×10^{12} cm^{-2} and mobility of 8000 cm^2/Vs at 5K.

Figure 6 shows the in-plane (s-polarized) and out-of-plane (p-polarized) intersubband absorption of the 31 Å QW sample. For QWs 25 Å to 45 Å wide,

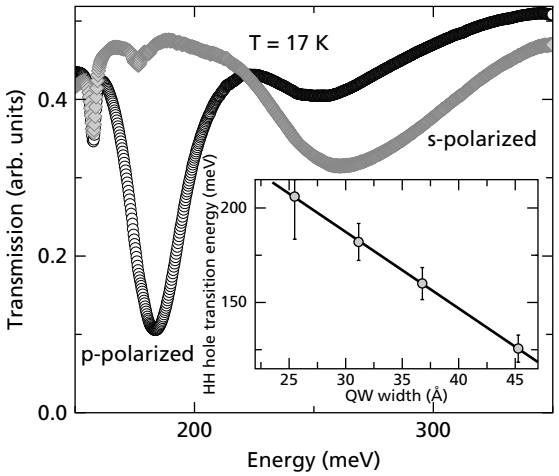

QW—Quantum well

The spectra for p-polarized (circles) and s-polarized (diamonds) light are shown for measurements at 17 K. The inset shows the heavy-to-heavy hole intersubband transition energies for 4 QW widths.

Figure 6.
Mid-infrared intersubband transmission spectra of a sample containing 31 Å wide, carbon modulation-doped GaAs QWs with digital $Al_{0.57}Ga_{0.43}As$ alloy barriers.

the absorption peak covers a broad mid-infrared range (i.e., 206 meV to 126 meV, ~6 μm to 10 μm wavelength) that is promising for application in quantum cascade emitters (see inset of Figure 6). Accurate simulations of valence-band structure are essential for the design of complex multi-QW QCL structure. We performed 6-band k · p calculations of the heavy-to-heavy hole transition energies considering the full band structure of the digitally alloyed barriers and found them to be in very good agreement with the experimental results for wider wells. The model is less accurate in predicting the out-of-plane absorption for the narrowest wells and the in-plane absorption features. For all practical purposes, however, the model is accurate enough to be adequate for band-structure calculations of hole QCL structures.

In this subsection we have been discussing only the GaAs system, but research on new QCL materials at Bell Labs also includes work on strained InGaAs/InAlAs on InP to access the low-wavelength mid-infrared range as well as investigations of the novel GaN system. Mid-infrared absorption measurements have been reported on GaN/AlGaN quantum wells [17, 18], and work is currently being done to study photocurrent and resonant tunneling.

Advanced Fabrication of InP-Based QCLs

In the section on device characterization, we introduced some of the main requirements for QCL applications that are still challenging for the technology: high-power operation, cw operation, and room-temperature operation. Our ongoing development to overcome these challenges involves designing high-performance structures, improving the quality of MBE material by improving the MBE process, and performing advanced device fabrication. MBE process improvement includes optimization of the doping level, growth parameters (e.g., temperature, growth rate, and arsenic overpressure), and a systematic effort to lower the defect level and unintentional background concentration. Advanced QCL fabrication includes epi-side-down mounting of the samples, HR-coating of the back facets, and InP overgrowth by either MBE or MOCVD.

MBE overgrowth has mainly been used to grow the top InP claddings or to create a buried grating for DFB lasers. However, both the thermal and optical properties of the deep-etched ridge waveguides can be improved dramatically by using a buried heterojunction design. In this case, the mesa patterning is done using an SiO_2 mask instead of photoresist. After the ridges have been wet-etched into the MBE-grown material, the wafer is transferred to an MOCVD reactor and a thick layer of InP is grown on the sides of the ridges (see schematics in **Figure 7**). MOCVD is the technique of choice for this process, because it allows selective-area overgrowth on the exposed semiconductor but not on the SiO_2 mask. The main benefit of this design is that it increases the heat dissipation out of the active region, allowing operation at higher currents and, consequently, higher maximum cw temperature. InP also has the advantage of a low refractive index that defines the lateral waveguide confinement. The losses of this geometry are lower than they are for deep-etched ridge waveguides, because the overlap of the wave with the metal top-contact is minimal. Figure 7 shows a cross-section of a device with InP overgrown on the sides of the ridge. The maximum cw operating temperature is increased by 25 K over that of a device without the buried heterojunction, and there is a total maximum cw temperature increase of 50 K when HR coatings are used on the back facet.

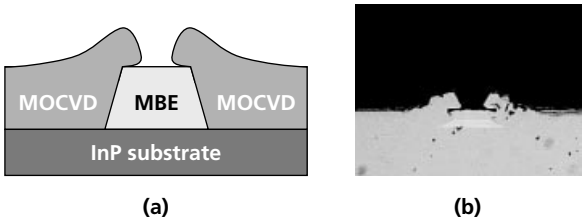

MBE—Molecular-beam epitaxy
MOCVD—Metal-organic chemical-vapor deposition

The lighter regions in **(b)** are the InGaAs (bottom) and InGaAs/InAlAs (top) MBE-grown QCL structure etched into a ridge-waveguide.

Figure 7.
Schematics of the InP MOCVD overgrowth process (a) and side image of a deep-etched ridge-waveguide (b) on which InP (darker regions) was grown by MOCVD.

Applications

The operating range of QCLs makes them ideal for chemical and biological sensing applications [25]. Most of the chemical compounds of interest for environmental or defense applications have absorption features in the mid-infrared. Their transmission through free atmosphere exhibits two windows (between 3 μm and 5 μm and between 8 μm and 13 μm) clear of water absorption. In these windows, strong absorption peaks have been identified for trace gasses, such as NO, NH_3, CH_4, and CO. Several spectroscopic techniques have been used to detect these gasses. The simplest method is direct absorption. In this setup, the change in intensity of a laser beam passing through a cell containing the target chemical is measured. The most commonly used optical method for trace-gas sensing is tunable infrared laser diode absorption spectroscopy (TILDAS). The high sensitivity and specificity of this technique is achieved by modulating the frequency of the laser so that it periodically scans through the absorption peak of the chemical of interest. The absorbing material converts the frequency modulation into an amplitude modulation that is detected by a lock-in technique. Recently, a lot of interest has been shown in photoacoustic trace-gas sensing. In the technique, the optical beam is periodically modulated in amplitude before illuminating the cell containing the absorbing chemical. The periodic heating of the chemical creates an acoustic wave that is detected with a microphone. This is a low-cost and sensitive technique that avoids the use of cooled mid-infrared detectors, but its sensitivity is typically limited by the laser power [23].

QCLs have so far been used in numerous spectroscopic studies for environmental purposes, health monitoring, and military applications. The first application of a thermoelectrically cooled DFB-QCL to continuous spectroscopic monitoring of CO in ambient air achieved a noise equivalent detection limit of 12 parts per billion (ppb) using a 102 cm optical path-length and a 2.5-minute data acquisition time at a 10 kHz pulsed-laser repetition rate [26]. **Figure 8** shows the CO concentration monitored in time over 14 hours with 10 ppb sensitivity. A spectroscopic gas sensor for nitric oxide (NO) detection based on a

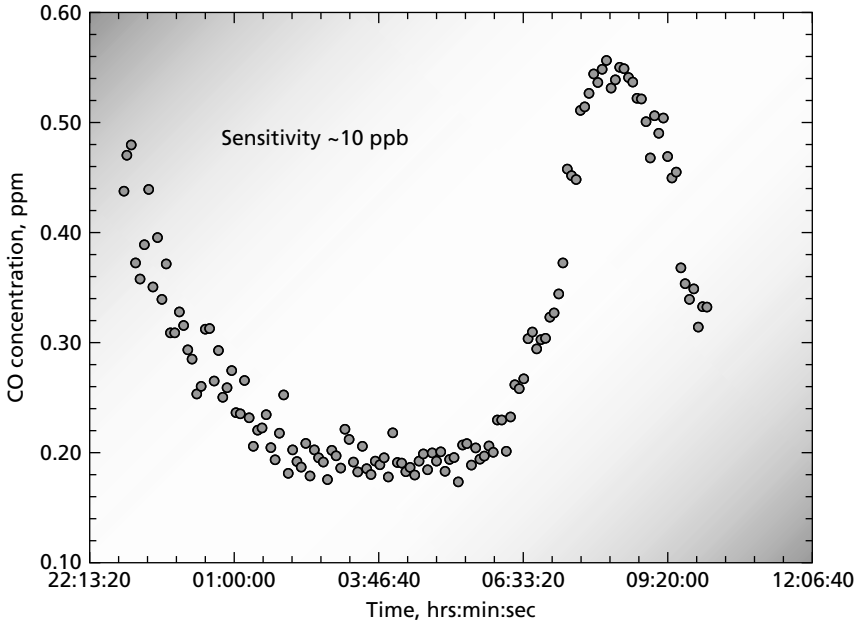

Figure 8.
CO concentration recorded over time in Houston, TX, with QCL spectroscopy.

cavity ringdown technique and a cw QC-DFB laser operating at 5.2 μm measured ppb NO concentrations in N_2 with a 0.7-ppb standard error [24]. NO detection is important for a number of applications, such as atmospheric pollution and toxic process monitoring, vehicle exhaust control, and noninvasive medical diagnostics. NO in exhaled breath is a possible biomarker for various lung diseases. Similarly, carbonyl sulfide (COS) in human breath has been related to liver and lung diseases. A detection sensitivity of 30 parts in 10^9 of COS and the selectivity of two stable isotopes has been demonstrated [36]. Other QCL spectroscopy studies include ammonia, methane, CO_2, and ethylene [41], to name just a few. Recently, a trace gas sensor based on quartz-enhanced photoacoustic spectroscopy with a QCL operating at 4.55 μm was developed for the detection of N_2O and CO and was found to have a sensitivity of 4 ppb for N_2O [23].

In addition to their use in *in situ* trace-gas sensing, QCLs could have an impact on remote sensing with LIDAR. Gittins et al. [13] used a multimode Fabry-Perot QCL operating at 8 μm for backscatter absorption measurements on isopropanol vapor. They explored the use of QCLs for differential-absorption LIDAR (DIAL) and found that even a simple configuration resulted in a detection limit of 12 ppm.

Another class of applications for which QCLs have strong potential to be of use is free-space optical communications. Because of lower Rayleigh and Mie scattering, the attenuation of mid-infrared light through open atmosphere is much lower than it is for visible or near-infrared light. Losses nearly one hundred times lower than those for shortwave infrared transmission can be expected in the second atmospheric window (i.e., 8 μm to 13 μm) in clear weather conditions. For lower visibility conditions, the advantage is even greater. An optical link based on QCL technology has been demonstrated to transmit audio, video, and data signals over 200 m at speeds up to 2.5 Gbit/s [30]. A unique feature of QCLs is their ultrafast carrier-relaxation lifetime (~1 ps), which is dominated by electron-optical phonon scattering. This property makes QCLs ideally suited for high-speed modulation. Active [33, 38] and passive [34] mode-locking has been achieved with QCLs and subpicosecond pulses have been produced with a repetition rate of 100 MHz to 10 GHz.

Conclusions

In the ten years since their invention, QCLs have evolved tremendously to reach all wavelengths from 3.7 μm to 24 μm. The success achieved with InP devices in the mid-infrared range was recently reproduced in the terahertz range with GaAs-based devices using the same general principles of intersubband light emission and electron transport [22]. The challenges for the technology now lie in the short-wavelength range. In the near-infrared range, several technologies are competing. We are exploring nonlinear light generation to extend the operation range of InP lattice-matched materials. In parallel with development to improve the performance of InP-based devices, we are investigating new materials and device concepts, including strained InGaAs/InAlAs on InP and hole QCLs in GaAs/AlGaAs. Completely novel material systems, such as GaN, may have to be developed in order to bridge the gap to telecommunications wavelengths.

The QCL devices operate either single- or multmode at temperatures well above 300 K. Multi-wavelength operation has also been achieved using either heterogeneous active regions or single cascades with giant nonlinear properties. Moreover, ultra-broadband emission in the 6 μm to 8 μm range has been demonstrated [19]. Currently there is a lot of interest in expanding these concepts to a broadband emitter that would simultaneously cover the entire mid-infrared range for sensing applications.

This paper has focused on Fabry-Perot and DFB QCL waveguides, but a significant amount of research has been done on other resonator cavities, such as microcavity and photonic crystal devices. Microcavity resonators are interesting because they are spectrally narrow, low-threshold, and low-noise laser sources. Whispering-cavity microdisc lasers, bow-tie lasers, and asymmetric cavity resonators have been studied for their unusual light-emitting patterns [1]. Most recently, a photonic crystal QCL has been demonstrated [4].

QCL technology has moved in a short time from research to production and QCLs are now a viable commercial alternative to other solid-state lasers. As compact, rugged, low-power-consumption light sources, QCLs are ideal candidates for applications, in particular for mobile field applications such as remote trace-gas sensing. The recent demonstration of high-power, room-temperature, cw QCL operation [8, 43] promises to significantly impact the sensing technologies. Moreover, QCLs also have potential for free-space optical communications, a field that has not yet been fully explored.

Acknowledgments

The authors would like to thank Jianxin Chen and Liming Zhang of Lucent Technologies for InP overgrowth by MBE and MOCVD, respectively. We also thank F. K. Tittel and A. A. Kosterev of Rice University for providing the CO spectroscopic data shown in Figure 8.

References

[1] Y. Baryshnikov, P. Heider, W. Parz, and V. Zharnitsky, "Whispering Gallery Modes Inside Asymmetric Resonant Cavities," Phys. Rev. Lett., 93 (2004), 133902-1–133902-4.

[2] I. Bormann, K. Brunner, S. Hackenbuchner, G. Zandler, G. Abstreiter, S. Schmult, and W. Wegscheider, "Midinfrared Intersubband Electroluminescence of Si/SiGe Quantum Cascade Structures," Appl. Phys. Lett., 80 (2002), 2260–2262.

[3] F. Capasso, C. Sirtori, and A. Y. Cho, "Coupled Quantum Well Semiconductors with Giant Electric Field Tunable Nonlinear Optical Properties in the Infrared," IEEE J. Quantum Electron., 30 (1994), 1313–1326.

[4] R. Colombelli, K. Srinivasan, M. Troccoli, O. Painter, C. F. Gmachl, D. M. Tennant, A. M. Sergent, D. L. Sivco, A. Y. Cho, and F. Capasso, "Quantum Cascade Surface-Emitting Photonic Crystal Laser," Science, 302 (2003) 1374–1377.

[5] G. Dehlinger, L. Diehl, U. Gennser, H. Sigg, J. Faist, K. Ensslin, D. Grützmacher, and E. Müller, "Intersubband Electroluminescence from Silicon-Based Quantum Cascade Structures," Science, 290 (2000), 2277–2280.

[6] L. Diehl, S. Mentese, E. Müller, D. Grützmacher, H. Sigg, U. Gennser, I. Sagnes, Y. Campidelli, O. Kermarrec, D. Bensahel, and J. Faist, "Electroluminescence from Strain-Compensated $Si_{0.2}Ge_{0.8}$/Si Quantum-Cascade Structures Based on a Bound-to-Continuum Transition," Appl. Phys. Lett., 81 (2002), 4700–4702.

[7] L. Diehl, H. Sigg, G. Dehlinger, D. Grützmacher, E. Müller, U. Gennser, I. Sagnes, T. Fromherz, Y. Campidelli, O. Kermarrec, D. Bensahel, and J. Faist, "Intersubband Absorption Performed on P-Type Modulation-Doped $Si_{0.2}Ge_{0.8}$/Si Quantum Wells Grown on $Si_{0.5}Ge_{0.5}$ Pseudosubstrate," Appl. Phys. Lett., 80 (2002), 3274–3276.

[8] A. Evans, J. S. Yu, S. Slivken, and M. Razeghi, "Continuous-Wave Operation of Lambda Similar to 4.8 μm Quantum-Cascade Lasers at Room Temperature," Appl. Phys. Lett., 85 (2004), 2166–2168.

[9] J. Faist, M. Beck, T. Aellen, and E. Gini, "Quantum-Cascade Lasers Based on a Bound-to-Continuum Transition," Appl. Phys. Lett., 78 (2001), 147–149.

[10] J. Faist, F. Capasso, C. Sirtori, D. L. Sivco, A. L. Hutchinson, and A. Y. Cho, "Laser Action by Tuning the Oscillator Strength," Nature, 386 (1997), 777–782.

[11] J. Faist, F. Capasso, D. L. Sivco, C. Sirtori, A. L. Hutchinson, and A. Y. Cho, "Quantum Cascade Laser," Science, 264 (1994), 553–556.

[12] J. Faist, C. Gmachl, M. Striccoli, C. Sirtori, F. Capasso, D. L. Sivco, and A. Y. Cho, "Quantum Cascade Disk Lasers," Appl. Phys. Lett., 69 (1996), 2456–2458.

[13] C. M. Gittins, E. T. Wetjen, C. Gmachl, F. Capasso, A. L. Hutchinson, D. L. Sivco, J. N. Baillargeon, and A. Y. Cho, "Quantitative Gas Sensing by Backscatter-Absorption Measurements of a Pseudorandom Code Modulated $\lambda \sim 8$ μm Quantum Cascade Laser," Appl. Opt., 25 (2000), 1162–1164.

[14] C. Gmachl, A. Belyanin, D. L. Sivco, V. Koncharovsky, M. L. Peabody, N. Owschimikow, A. M. Sergent, F. Capasso, and A. Y. Cho, "Optimized Second-Harmonic Generation in Quantum Cascade Lasers," IEEE J. Quantum Electron., 39 (2003), 1345–1355.

[15] C. Gmachl, F. Capasso, D. L. Sivco, and A. Y. Cho, "Recent Progress in Quantum Cascade Lasers and Applications," Rep. Prog. Phys., 64 (2001), 1533–1601.

[16] C. Gmachl, J. Faist, F. Capasso, C. Sirtori, D. L. Sivco, and A. Y. Cho, "Long-Wavelength (9.5–11.5 μm) Microdisk Quantum-Cascade Lasers," IEEE J. Quantum Electron., 33 (1997), 1567–1573.

[17] C. Gmachl and H. M. Ng, "Intersubband Absorption at $\lambda \sim 2.1$ μm in A-Plane GaN/AlN Multiple Quantum Wells," Electron. Lett., 39 (2003), 567–569.

[18] C. Gmachl, H. M. Ng, and A. Y. Cho, "Intersubband Absorption in Degenerately Doped GaN/$Al_xGa_{1-x}N$ Coupled Double Quantum Wells," Appl. Phys. Lett., 79 (2001), 1590–1592.

[19] C. Gmachl, D. L. Sivco, R. Colombelli, F. Capasso, and A. Y. Cho, "Ultra-Broadband Semiconductor Laser," Nature, 415 (2002), 883–887.

[20] R. P. Green, A. Krysa, J. S. Roberts, D. G. Revin, L. R. Wilson, E. A. Zibik, W. H. Ng, and J. W. Cockburn, "Room-Temperature Operation of InGaAs/AlInAs Quantum Cascade Lasers Grown by Metalorganic Vapor Phase Epitaxy," Appl. Phys. Lett., 83 (2003), 1921–1922.

[21] M. K. Gurnick and T. A. De Temple, "Synthetic Nonlinear Semiconductors," IEEE J. Quantum Electr., 19 (1983), 791–894.

[22] R. Kühler, A. Tredicucci, F. Beltram, H. E. Beere, E. H. Linfield, A. G. Davies, D. A. Ritchie, R. C. Iotti, and F. Rossi, "Terahertz Semiconductor-Heterostructure Laser," Nature, 417 (2002), 156–159.

[23] A. A. Kosterev, Y. A. Bakhirkin, and F. K. Tittel, "Ultrasensitive Gas Detection by Quartz-Enhanced Photoacoustic Spectroscopy in the Fundamental Molecular Absorption Bands Region," Appl. Phys. B, 80 (2005), 133–138.

[24] A. A. Kosterev, A. L. Malinovsky, F. K. Tittel, C. Gmachl, F. Capasso, D. L. Sivco, J. N. Baillargeon, A. L. Hutchinson, and A. Y. Cho, "Cavity Ringdown Spectroscopic Detection of Nitric Oxide with a Continuous-Wave Quantum-Cascade Laser," Appl. Opt., 40 (2001), 5522–5529.

[25] A. A. Kosterev and F. K. Tittel, "Chemical Sensors Based on Quantum Cascade Lasers," IEEE J. Quantum Electron., 38 (2002), 582–591.

[26] A. A. Kosterev, F. K. Tittel, R. Köhler, C. Gmachl, F. Capasso, D. L. Sivco, A. Y. Cho, S. Wehe, and M. G. Allen, "Thermoelectrically Cooled Quantum Cascade Laser-Based Sensor for the Continuous Monitoring of Ambient Atmospheric Carbon Monoxide," Appl. Opt., 41 (2002), 1169–1173.

[27] O. Malis, A. Belyanin, C. Gmachl, D. L. Sivco, M. L. Peabody, A. M. Sergent, and A. Y. Cho, "Improvement of Second-Harmonic Generation in Quantum Cascade Lasers with True Phase Matching," Appl. Phys. Lett., 84 (2004), 2721–2723.

[28] O. Malis, A. Belyanin, D. L. Sivco, J. Chen, A. M. Sergent, C. Gmachl, and A. Y. Cho, "Milliwatt Second-Harmonic Generation in Quantum-Cascade Lasers with Modal Phase-Matching," Electron. Lett., 40 (2004), 1586–1587.

[29] O. Malis, A. Belyanin, D. L. Sivco, J. Chen, A. M. Sergent, C. Gmachl, and A. Y. Cho, "Recent Progress in Nonlinear Quantum Cascade Lasers," SPIE Proceedings of Photonics West, forthcoming in 2005.

[30] R. Martini, C. Gmachl, J. Falciglia, F. G. Curti, C. G. Bethea, F. Capasso, E. A. Whittaker, R. Paiella, A. Tredicucci, A. L. Hutchinson, D. L. Sivco, and A. Y. Cho, "High-Speed Modulation and Free-Space Optical Audio/Video Transmission Using Quantum Cascade Lasers," Electron. Lett., 37 (2001), 192–193.

[31] T. S. Mosely, A. Belyanin, C. Gmachl, D. L. Sivco, M. L. Peabody, and A. Y. Cho, "Third Harmonic Generation in a Quantum Cascade Lasers with Monolithically Integrated Resonant Optical Nonlinearity," Optics Express, 12 (2004), 2972–2976.

[32] N. Owschimikow, C. Gmachl, A. Belyanin, V. Kocharovsky, D. L. Sivco, R. Colombelli, F. Capasso, and A. Y. Cho, "Resonant Second-Order Nonlinear Optical Processes in Quantum Cascade Lasers," Phys. Rev. Lett., 90 (2003), 043902-1–043902-4.

[33] R. Paiella, F. Capasso, C. Gmachl, H. Y. Hwang, D. L. Sivco, A. L. Hutchinson, A. Y. Cho, and H. C. Liu, "Monolithic Active Mode Locking of Quantum Cascade Lasers," Appl. Phys. Lett., 77 (2000), 169–171.

[34] R. Paiella, F. Capasso, C. Gmachl, D. L. Sivco, J. N. Baillargeon, A. L. Hutchinson, A. Y. Cho, and H. C. Liu, "Self-Mode-Locking of Quantum Cascade Lasers with Giant Ultrafast Optical Nonlinearities," Science, 290 (2000), 1739–1742.

[35] J. S. Roberts, R. P. Green, L. R. Wilson, E. A. Zibik, D. G. Revin, J. W. Cockburn, and R. J. Airey, "Quantum Cascade Lasers Grown by Metalorganic Vapor Phase Epitaxy," Appl. Phys. Lett., 82 (2003), 4221–4223.

[36] C. Roller, A. A. Kosterev, F. K. Tittel, K. Uehara, C. Gmachl, and D. L. Sivco, "Carbonyl Sulfide

Detection with a Thermoelectrically Cooled Midinfrared Quantum Cascade Laser," Optics Lett., 28 (2003), 2052–2054.
[37] C. Sirtori, H. Page, C. Becker, and V. Ortiz, "GaAs-AlGaAs Quantum Cascade Lasers: Physics, Technology, and Prospects," IEEE J. Quantum Electron, 38 (2002), 547–558.
[38] A. Soibel, F. Capasso, C. Gmachl, M. L. Peabody, A. M. Sergent, R. Paiella, H. Y. Hwang, D. L. Sivco, A. Y. Cho, H. C. Liu, C. Jirauschek, and F. X. Kartner, "Active Mode Locking of Broadband Quantum Cascade Lasers," IEEE J. Quantum Electron., 40 (2004), 844–851.
[39] F. Szmulowicz and G. J. Brown, "Calculation and Photoresponse Measurement of the Bound-to-Continuum Infrared Absorption in P-Type GaAs/$Al_xGa_{1-x}As$ Quantum Wells," Phys. Rev. B, 51 (1995), 13203–13220.
[40] A. Tredicucci, C. Gmachl, F. Capasso, D. L. Sivco, A. L. Hutchinson, and A. Y. Cho, "Long Wavelength Superlattice Quantum Cascade Lasers at 17 μm," Appl. Phys. Lett., 74 (1999), 638–640.
[41] D. Weidmann, A. A. Kosterev, C. Roller, R. F. Curl, M. P. Fraser, and F. K. Tittel, "Monitoring of Ethylene by a Pulsed Quantum Cascade Laser," Appl. Opt., 43 (2004), 3329–3334.
[42] L. R. Wilson, D. A. Carder, J. W. Cockburn, R. P. Green, D. G. Revin, M. J. Steer, M. Hopkinson, G. Hill, and R. Airey, "Intervalley Scattering in GaAs-AlAs Quantum Cascade Lasers," Appl. Phys. Lett., 81 (2002), 1378–1380.
[43] J. S. Yu, A. Evans, J. David, L. Doris, S. Slivken, and M. Razeghi, "High-Power Continuous-Wave Operation of Quantum-Cascade Lasers up to 60 C," IEEE Photon. Tech. Lett., 16 (2004), 747–749.

(Manuscript approved May 2005)

OANA MALIS is a research consultant in the Semiconductor Physics Research Department at Bell Labs in Murray Hill, New Jersey. She has an M.S. degree in physics from the University of Bucharest in Romania and a Ph.D. degree in physics from Boston University in Massachusetts. Dr. Malis is currently leading the Lucent research and development in mid-infrared intersubband semiconductor lasers. Her professional interests include the characterization of the optical and electronic properties of novel semiconductor materials.

CLAIRE GMACHL is an associate professor in the Electrical Engineering Department at Princeton University in New Jersey. Before joining the faculty at Princeton, she was a distinguished member of technical staff at Bell Labs in Murray Hill, New Jersey. She has an M.S. degree in physics from the University of Innsbruck in Austria and a Ph.D. degree in electrical engineering from the Technical University of Vienna, also in Austria. Dr. Gmachl has demonstrated many innovative QCL concepts, such as bidirectional, multiwavelength, and broadband QCLS, and, recently, nonlinear light generation in QCLs. Other key contributions include the development of single-mode and tunable-distributed-feedback QCLs and chaotic micro-cavity lasers with high optical power and directionality. Her professional interests include research and education in electrical engineering, with a focus on optics and optical electronics. Dr. Gmachl is a member of the 2002 TR100 and is a 2002/03 IEEE/LEOS Distinguished Lecturer. She is a recipient of the 2003 Snell Premium award of the IEEE, the 2000 NASA Group Achievement Award, the 1996 Solid State Physics Award of the Austrian Physical Society, and the 1995 Christian Doppler Award of Austria. She is a senior member of the IEEE and LEOS.

DEBORAH L. SIVCO is a member of technical staff in the Semiconductor Physics Research Department at Bell Labs in Murray Hill, New Jersey. She has a B.S. degree in chemistry from Rutgers University in New Brunswick, New Jersey, and an M.S. in materials science from Stevens Institute of Technology in Hoboken, New Jersey. She has been working on the molecular beam epitaxy (MBE) growth of III–V compounds since 1981. In 1994, she prepared the world's first quantum cascade laser, in collaboration with Faist, et. al. Her professional interests include the fabrication of advanced mid-infrared light sources and detectors, in particular quantum cascade lasers. She is a co-recipient of the 1994 Newcomb Cleveland Prize, the 1995 British Electronic Letters Premium Award, the 1996 Technology of the Year Award of Industry Week *magazine, and the 2000 NASA Group Achievement Award.*

LOREN N. PFEIFFER is a distinguished member of

technical staff in the Semiconductor Physics Research Department at Bell Labs in Murray Hill, New Jersey. He received his B.S. degree in physics from the University of Michigan in Ann Arbor and his Ph.D., also in physics, from The Johns Hopkins University in Baltimore, Maryland. A world-renowned leader in the field of molecular beam epitaxy (MBE) technology, he is currently focusing on high-purity growth of GaAs/AlGaAs quantum well heterostructures. His devices have been proven to exhibit the highest electron mobility ever reported for any semiconductor. His professional interests include ultra-clean semiconductor growth using MBE, as well as studies of quantum wires, quantum dots, and other nanoscale structures with novel properties. Dr. Pfeiffer is a fellow of both the American Physical Society and the Johns Hopkins Society of Scholars, and he is the recipient of the 2004 McGroddy Prize of the American Physical Society.

A. MICHAEL SERGENT is a member of technical staff in

the Condensed Matter Physics Research Department at Bell Labs in Murray Hill, New Jersey. He is currently involved in the development of new processing techniques for quantum cascade lasers and contacting Pentacene single crystals for defect studies. He also supports the GaN molecular beam epitaxy group at Bell Labs, where his efforts focus on improving MBE technology and developing insulated-gate Hall bar structures for low-temperature transport studies of AlGaN/GaN heterostructures.

KENNETH W. WEST is a member of technical staff in the

Semiconductor Physics Research Department at Bell Labs in Murray Hill, New Jersey. He is currently working on the growth and characterization of novel semiconductor structures. His professional interests include development of new molecular beam epitaxy processes for high-purity semiconductor structures. He holds a B.S. degree in physics from Bucknell University in Lewisburg, Pennsylvania. ◆